Investigation of microstructural damage to eutectic carbides from scratch tests of a heat-treated Fe-Cr-W-Mo-V-C alloy

Jing Guo[a,b], Yunli Feng[a], Ligang Liu[b], Xiaolei Xing[b], Xuejun Ren[c], Qingxiang Yang[b,*]

[a] *College of Metallurgy and Energy, North China University of Science and Technology, Tangshan 063009, China*

[b] *State Key Laboratory of Metastable Materials Science & Technology, Yanshan University, Qinhuangdao 066004, China*

[c] *School of Engineering, Liverpool John Moores University, Liverpool L3 3AF, UK*

*Corresponding author: Tel. +86-335-838-7471

Fax. +86-335-807-4545

E-mail address: qxyang@ysu.edu.cn, guojing@ysu.edu.cn

Abstract: The characteristics of abrasive wear damage to the carbides and eutectic phases in a Fe-Cr-W-Mo-V-C alloy were systematically investigated using point scratch testing on heat-treated samples with preserved eutectic structures from a characteristic eutectic carbide formation temperature of 1240°C. A deep-etching method is applied to study the detailed morphologies of the eutectic carbides by optical microscopy (OM) and field emission scanning electron microscopy (FESEM). The types of the eutectic carbides was identified by X-ray diffraction (XRD) as V-rich eutectic MC and Mo-rich eutectic M_2C. Single-pass scratch tests were carried out on polished and deep-etched surfaces of the specimens to investigate the micro-scale wear behavior of the eutectic carbides with and without protection by the matrix phase. It was found that, when a surrounding matrix is present, the micro-cracks initiate from the eutectic region during the scratch tests and slip-lines appear in scratched edges of the matrix phase. Without matrix protection as revealed in the deep etched samples, the main failure form is carbide dendrites break-off forming wear debris. The detailed differences in response and deformation mode of carbide microstructures with/without matrix support to single-point abrasion behavior are schematically depicted for main eutectic MC and M_2C carbides under different loading conditions. Potential

improvement on wear performance through the composition design is also discussed based on the different fracture and wear behavior of V-rich eutectic MC and Mo-rich eutectic M_2C identified.**Keywords:** Eutectic carbide; Abrasive wear; Scratch; Crack initiation; Crack propagation

1 Introduction

Fe-Cr-W-Mo-V-C alloy is an advanced steel alloy with high hardness, wear resistance and good hardenability [1]. There are several types of carbide in this alloy system with different morphologies and compositions formed during the primary and eutectic transformation. Recently, Fe-Cr-W-Mo-V-C alloy has been used to replace the traditional cold work roll materials [2], for this application abrasive wear is the main failure mechanism of the cold work roll in service [3-5]. During the abrasive wear process, the carbides in the alloy play a significant role in the wear resistance of the cold work roll [6-9].

The function of carbides in abrasive wear processes and interaction between carbide and matrix has been studied in several research works. L.S Zhong et al found that the relative wear resistance of particulate–reinforced iron matrix composites is increased initially and then decreased with increasing volume fraction of V_8C_7 [10]. Y.P. Ji et al demonstrated that the primary VC carbide size and the mean distance can significantly influence the wear resistance of high vanadium high speed steel [11]. A. Bedolla-Jacuinde et al suggested that primary MC and eutectic M_7C_3 in the high-chromium white irons strengthen the matrix, and the strengthening of the matrix in turn provides better support to the eutectic carbides against cracking [12]. Due to the omplex nature of carbides in steel, in most cases, researchers can only generally link the wear behavior of a material with the size, quantity, distribution and orientation of the carbide's and deduce the operative role and influence of carbides during the wear process [13-17]. Works on the wear behavior of the carbide itself with

well-defined conditions have been rarely reported. It is of significant importance to establish the wear behavior and mechanism of the carbides to fundamentally understand the contribution that carbides make to the whole matrix, which in turn would provide more direct information for structure improvement and alloy composition design for wear performance improvement.

According to a previous study [18] on the phase structure of Fe-Cr-W-Mo-V-C alloy, the eutectic carbides (primary carbide) form first, then followed by secondary carbides during the solidification process. The type, morphology and evolution process of the eutectic carbide has a significant impact on the structure of the secondary carbide and the carbides in the final as-cast organisation [19,20]. There are very fewreports which has been focused on the wear behavior of the eutectic carbide. Compared to the volume of the matrix, the fraction of the carbide in Fe-Cr-W-Mo-V-C alloy is much lower , this make it difficult to directly observe the wear behavior of the carbide by general macroscopic experimental methods.In this work, scratch test was carried out on a heat-treated Fe-Cr-W-Mo-V-C alloy (with preserved carbide structures) by micron-level CSM Revetest Xpress Scratch Tester, which is often used for testing and analyse thin-film materials.[21-23]. The wear behavior of the eutectic carbide with matrix support on the micro scale was investigated by the single-pass scratch tests. Selected specimen was deep etched to remove the matrix in order to investigate the wear behavior of the eutectic carbide without matrix protection.

2 Experimental details

The specimens were taken from a self-designed Fe-Cr-W-Mo-V-C alloy for cold work roll, the chemical composition of the alloy is listed in Table 1.

Table 1 Chemical compositions of the alloy (wt %)

Element	C	Cr	Mo	V	W	Mn	Si	Fe
Content	1.14	10	3.5	2.6	0.5	0.2	0.5	Bal.

According to a previous study, during the solidification process of Fe-Cr-W-Mo-V-C

alloy, the eutectic reaction occurs at 1253°C forming a microstructure consists of austenite and eutectic carbides. Considering sufficient undercooling, 1240°C was chosen as the characteristic temperature in the work. The specimens were firstly heated up to 1400°C and held for 10 min, then cooled slowly to 1240°C in furnace, and quenched quickly in water to fix the microstructures.

The specimens were polished and color etched in Murakami etchant [24] (3g $K_3Fe(CN)_6$ + 10g NaOH + 100ml H_2O), and then observed with a Axiovert 200 MAT optical microscope (OM). Additionally, some specimens were soaked for about 30min (deep-etching treatment) in 5g $FeCl_3$ + 10ml HNO_3 + 3ml HCl + 87ml ethylalcohol [25] to observe the deep-etched morphology of the eutectic carbide on a S4800-II Field Emission Scanning Electron Microscope (FESEM) and determine the phase structures by D/max-2500/PC X-Ray Diffractometer (XRD).

Single-pass scratch tests were carried out on a CSM Revetest Xpress Scratch Tester employing a conical diamond indenter with a hemispherical tip, the radius of the indenter tip is 100μm. Both as-polished samples and deep etched samples were tested under comparable conditions to investigate the wear behavior of the eutectic carbide with and without the matrix protection. During the single-pass scratch tests, scratches (~5mm long) were conducted at a speed of 6mm/min with five different constant loads of 1, 5, 10, 15 and 20N. The residual scratch tracks were observed on SEM to reveal the wear behavior and fracture patterns of the eutectic carbides. The distribution of key elements on the surface of the scratch was analyzed by Energy Dispersive Spectroscopy (EDS).

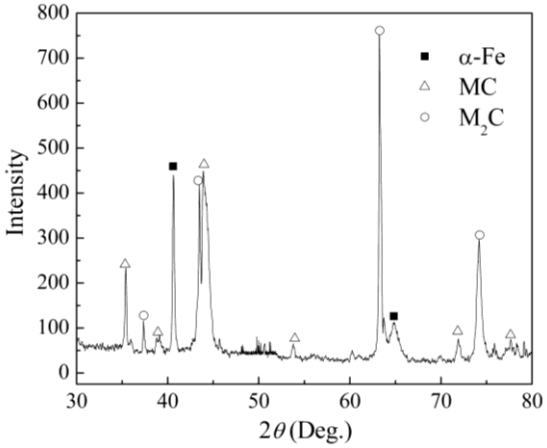

Fig.1 XRD pattern of deep-etched sample.

3 Results

3.1 XRD analysis and microstructure

Fig.1 shows the XRD pattern of the deep-etched specimen after quenching from 1240°C. It is clearly shown that α–Fe (martensite), MC and M_2C exist in the alloy. Based on the Fe–C isopleths reported in a previous study [18], the ternary eutectic reaction, L→γ+MC+M_2C, occurs at 1240°C and the microstructure consists of austenite (γ–Fe), eutectic MC and eutectic M_2C. When the specimen is quenched from this temperature, the austenite transforms into martensite, which appears in the form of α–Fe in the XRD pattern.

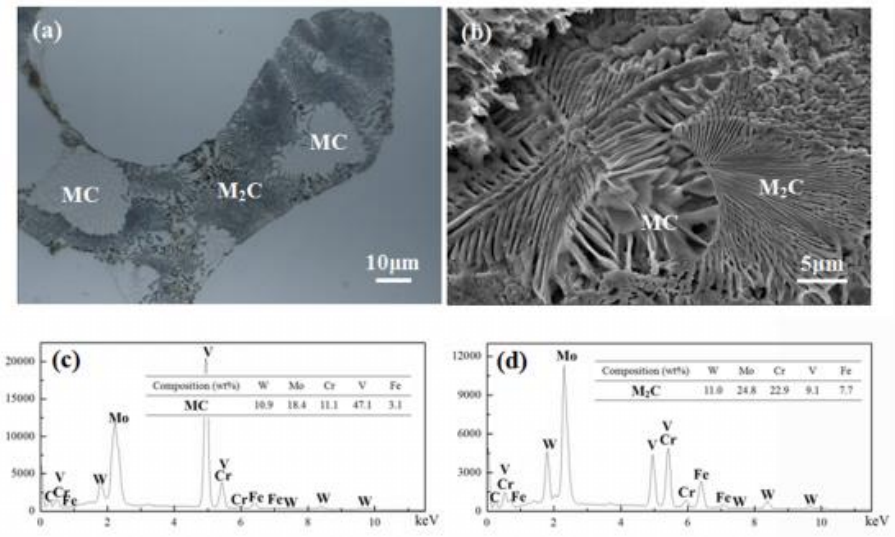

Fig.2 Two-dimensional (a) and deep-etched (b) morphologies of eutectic carbides; EDS analyses of (c) eutectic MC and (d) eutectic M_2C.

Fig.2 shows the microstructure of the eutectic carbide in the quenched specimen. From

Fig.2(a), the eutectic carbide is etched into two different colors by Murakami etchant, which represents two kinds of carbides. The black part is fibrous–like eutectic M_2C, and the gray one is eutectic MC, which distributes sparsely. As shown in the figure, these two types of carbides mix together and grow along the crystal grain boundaries. The morphologies of the eutectic carbide after deep etching is shown Fig.2(b). It can be seen that the morphologies of the eutectic MC and M_2C are quite different. The eutectic MC is relatively large and grows dispersedly with a random structural feature inside, whereas the eutectic M_2C is of closely arranged finer feature. Observation of the cross–section reveals that the M_2C is of a fibrous shape. Fig.2(c) and 2(d) are EDS results of eutectic MC and M_2C, respectivly. The data clearly shows that eutectic MC is a V-rich carbide, while eutectic M_2C is rich in element Mo, accompanied by a certain amount of Cr, these are consistent with chemical compositions of MC and M_2C reported in other studies [19,20].

3.2 Micro-wear behavior of eutectic carbides with matrix protection

Typical constant load scratch patterns on the polished surfaces of the quenched specimen with five different loads are presented in Fig.3. The red arrows represent the indenter sliding direction. Fig.3(a) shows the starting end where the indenter begin the scratch with a load of 1N, while Fig.3(b)-(e) show the finishing end of the scratch with a load of 5, 10, 15 and 20 N, respectively. From Fig.3, the width of the scratches increases from 25μm to 65μm with increasingload. There is a clear built-up zone at the edge and exiting end of the scratch where the wear debris accumulate. As the load is over 10N, the secondary plowing starts to appear, which is caused by continued scratching of the peeling wear debris (see Fig.3(c)-(e)). A close-up view of edge of the scratch for loads of 5N and 20N is shown in Fig.4. The boundaries of the scratch groove are indicated by white dotted lines. It is clearly shown on Fig.4(a), plastic deformation occurs at the scratched edge causing apparent matrix uplift at 5N, whereas the eutectic carbide retains the original dendrite feather without obvious

deformation and micro-cracks. From Fig.4(b), much more severe plastic deformation could be observed at the scratch with a load of 20N. The slip-lines appear at the scratched edge of the matrix phase, which are parallel to each other and oriented at an angle to the scratch direction or intersected with other sets of slip-lines. It indicates that the micro-cracks also appear within the eutectic carbide.

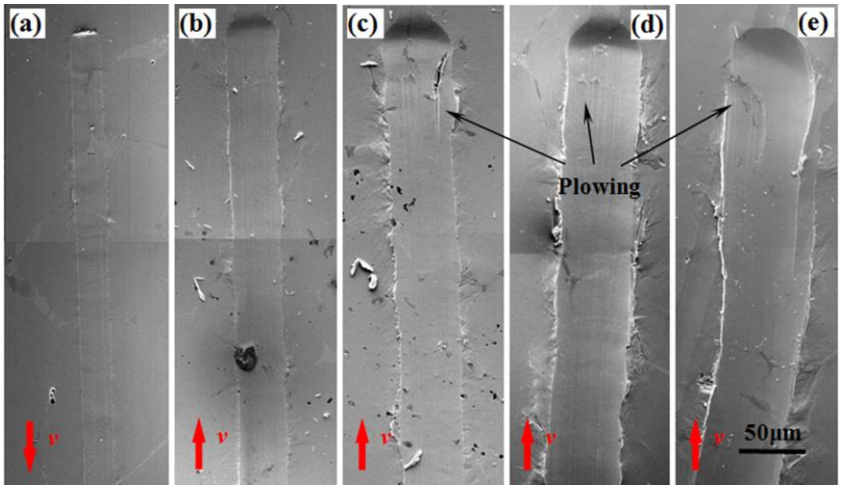

Fig.3 Scratch profiles on the polished surface of specimen at a load of (a) 1 N, (b) 5 N, (c) 10 N, (d) 15 N and (e) 20 N.

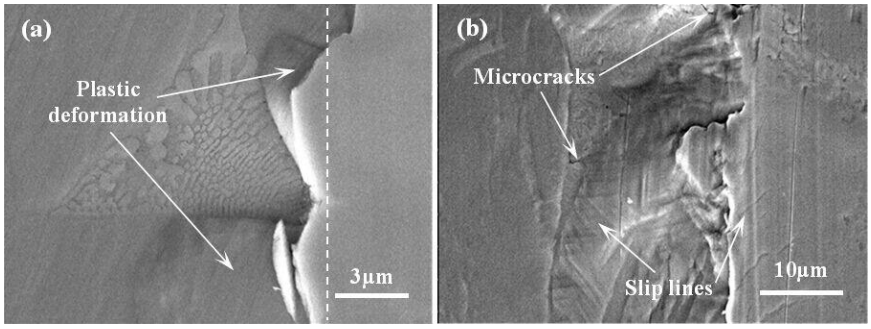

Fig.4 Micrographs showingscratch-induced deformation near the edge at a load of (a) 5 N and (b) 20 N.

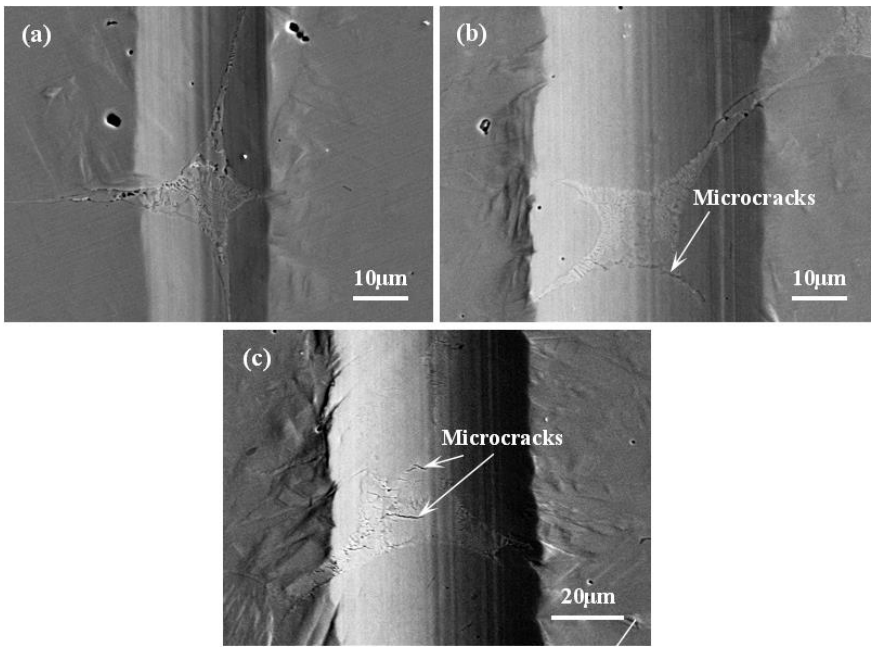

Fig.5 SEM micrographs of eutectic carbides within the scratch groove at a load of (a) 1N, (b) 5N and (c) 10N.

Fig.5 are SEM micrographs showing the eutectic carbide within the scratch grooves at 1N, 5N and 10N. It can be clearly seen that the dendrite feather of the eutectic carbide is not changed, which indicates that the indenter only micro-cut the specimen's surface. With increase of the load, the micro-cracks could be observed to have initiated from the eutectic region. From Fig.5(a), no micro-crack could be observed within the eutectic carbide at 1N, while micro-cracks less than 1μm in length start to appear in the eutectic region at 5N as revealed in Fig.5(b). The micro-cracks in the eutectic region enlarges gradually as the load continues to increase. At 10N, the micro-cracks larger than 10μm in length can be observed in Fig.5(c). The micro-cracks in the scratch groove are approximately perpendicular to the sliding direction. The micro-cracks within the eutectic carbide are further analysed by classifying them into the intergranular and transgranular cracks. In this work, intergranular crack refers to the crack that appears at the carbide-boundary. When the dendrite spacing is small enough, the intergranular cracks of the adjacent dendrites connect to each other and propagate to form a large crack, even longer than a few dozen microns, which mostly exists on the edge of eutectic region (see Fig.6(a)). Transgranular crack is defined as the internal

crack, which crosses through the carbide dendrite. This crack is relatively small and only propagates across a few dendrites (see Fig.6(b)).

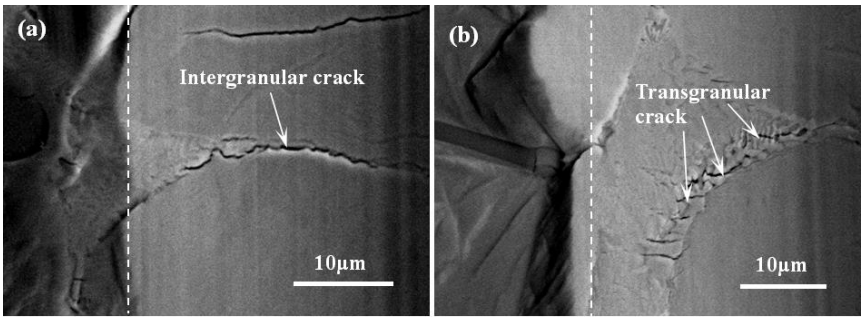

Fig.6 Microcracks within the eutectic carbide classified into (a) intergranular crack and (b) transgranular crack.

Back-scattered electron (BSE) imaging method was adopted in this work to distinguish the micro-crack morphologies in different eutectic regions as shown in Fig.7. In eutectic MC, most of micro-cracks are transgranular ones. Due to the large dendrite size and spacing, as well as different dendrite orientation in the MC cluster, the micro-cracks hardly coalescence and propagate. Clearly, both transgranular cracks and intergranular cracks can be observed in the M_2C cluster.. From Fig.7, transgranular crack can be found in Area A within the M_2C cluster across only a few dendrites. In Area B, intergranular cracks on the edge of M_2C cluster connect to each other and form a large crack over 1μm width and a few dozen microns long. When the intergranular crack grows into the M_2C cluster (see Area C in Fig.7), the crack propagates slowly and terminates eventually. When the intergranular crack forms on the M_2C dendrite in the transition zone between the clusters, it does not propagate at all (see Area D in Fig.7). Combined the observation in Figs.5, 6 and 7, it is reasonable to consider that the observed micro-cracks only appear in the eutectic region and propagate inside or between the carbide clusters.

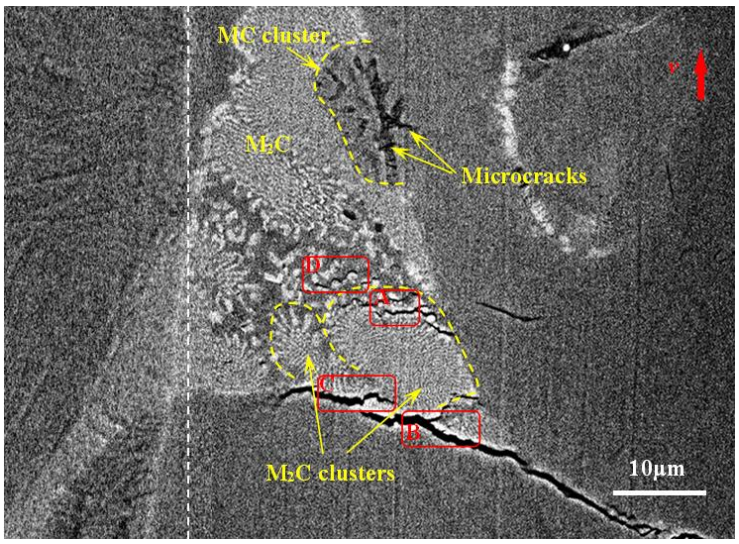

Fig.7 Back-scattered electron (BSE) image of eutectic carbides within the scratch groove at a load of 20N.

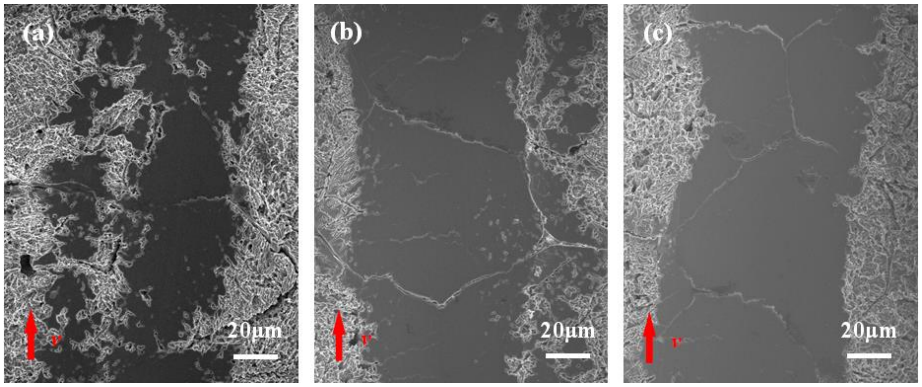

Fig.8 Scratch profiles on the deep-etched surface of specimen at a load of (a) 5 N, (b) 15 N and (c) 20 N.

3.3 Micro-wear behavior of the eutectic carbide without matrix protection

Fig.8 shows the morphological images of the scratch on deep-etched specimens with different loads. The width of the scratch increases with higher applied load, and the carbide boundaries within the scratch become much clearer. By comparison with corresponding polished specimen at comparable same loads in Fig.3, the width of the scratch is found to have increased significantly. As shown in Fig.8(a), the scratch at 5N is not smooth, and there is a large area of etching trace. As the load increases beyond 15N, the etching trace in the groove disappears gradually, and the boundary of the groove becomes much clearer (see Fig.8(b)-(c)).

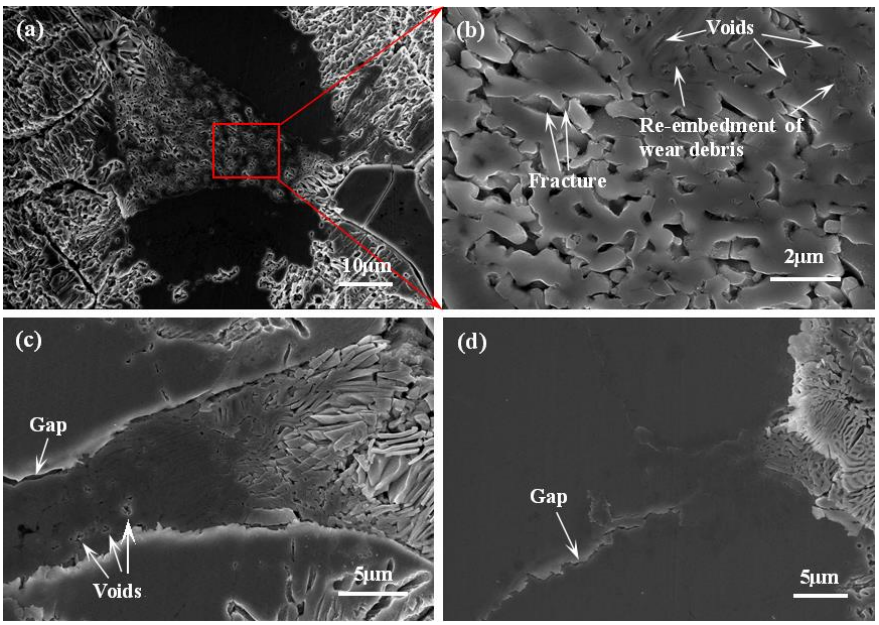

Fig.9 SEM micrographs of eutectic carbides within the scratch groove (deep-etched) at a load of (a-b) 1 N, (c) 5 N and (d) 10 N. (b) is a close-up view of (a).

SEM micrographs in Fig.9 show the eutectic carbide in the scratch groove of deep-etched specimens at 1N, 5N and 10N. From Fig.9(a), the eutectic carbides are clearly visible in the sample with an applied load of 1N bulging out of the matrix. Fig.9(b) shows a partially enlarged view of a selected region (red box) in Fig.9(a) revealing an unchanged dendrite feature of the eutectic carbide. However, compared to the original undeformed morphology, the dendrite width of the eutectic carbide is larger, while the dendrite spacing is smaller. This is probably associated with by re-embedment of wear debris of carbide dendrite. Some cracks with random directions could also be observed appearing within the carbide dendrites. In Fig.9(c), the dendrite feather of the eutectic carbide in the center of groove totally disappears at 5N. The eutectic carbide is pressed into the matrix, and only limited numbers of voids remain in the eutectic region that can be used to distinguish the adjacent carbide dendrites. The gap between the matrix and eutectic region can also be seen in Fig.9(c) to determine the location of the eutectic carbide and the width of the eutectic region.Near the edge of the scratch groove, three–dimensional morphology of the eutectic carbide dendrite can be observed. The carbide dendrites that bulged out of the matrix fall

down along the sliding direction, and are seriously fractured along the cross-section planeof the dendrite. Some of the fractured dendrites are detached from the matrix and become wear debris, and others are pressed on top of the fractured dendrites ahead. From Fig.9(d), the eutectic carbides in the groove are completely pressed into the matrix with an applied load of 10N and separated from those on the side of scratch. The deformation direction of the eutectic carbide can only be inferred by the gap between the matrix and eutectic region. Also at 10N, the whole eutectic region are found to have fractured outside the scratch groove and move upward as shown in Fig.10. A magnified view of the fracture surface is also shown in Fig. 10. . It can be clearly seen that all the carbide dendrites on the longitudinal section are fractured forming flake or granular debris.Once the debris enters into the scratch area, it is either being pressed into the matrix, or in the rolling state, forming a three-body abrasive wear system.

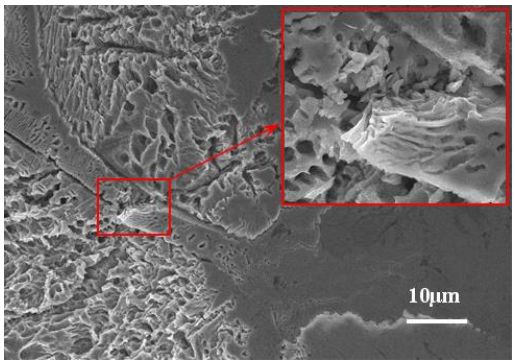

Fig.10 Fracture morphology of eutectic carbides outside the scratch groove at 10 N (deep-etched).

As the load is increased beyond 10N, it can be seen from Fig.8 and Fig.9 that it is difficult to determine the location and wear behavior of the eutectic carbide from the smooth groove formedby the indenter. So EDS surface analysis was adopted here to determine the distribution of the eutectic carbides in order to establish their wear behavior when there is no matrix protection. In this alloy, a large amount of element Cr exist in the matrix, which seriously disturb the EDS results. Meanwhile, the eutectic MC and M_2C are V- and Mo-rich carbides, respectively, without too much element Cr. Therefore, the element Cr can be

ignored and unselected during the EDS analysis. Fig.11 is SEM images and corresponding EDS analyses on the deep-etched specimen at 15N. From Fig.11(a), the full length of the eutectic carbide along the grain boundary within the groove is interrupted by scratch, but EDS could clearly prove the continued feature of the carbide as shown in Fig.11(b). In Fig.11(b), the area of the eutectic region along the grain boundary within the groove as represented by Area A is enlarged , which indicates that the carbide dendrites are fractured and then pressed into matrix on (next to) the original site of the carbide feather.. Area B is located inside the eutectic region and shows apparent enrichment of elements V and Mo, which reveals that the fractured dendrites become the wear debris and are pressed into the matrix in other regions. Also at 15N, both SEM and EDS results (Fig.11(c)-(d)) show the disconnection of the eutectic carbide in the scratch groove, which demonstrates that the carbide dendrites are displaced from their roots by the indenter and eventually become part of the wear debris. The dimension the wear debris is generally on the dendrite scale with small sizes. There is also some wear debris of the eutectic carbide on the cluster scale found on the deep-etched specimen at 20N (see Fig.12), which retains the original deep-etched dendrite morphology with a size of ~10μm.

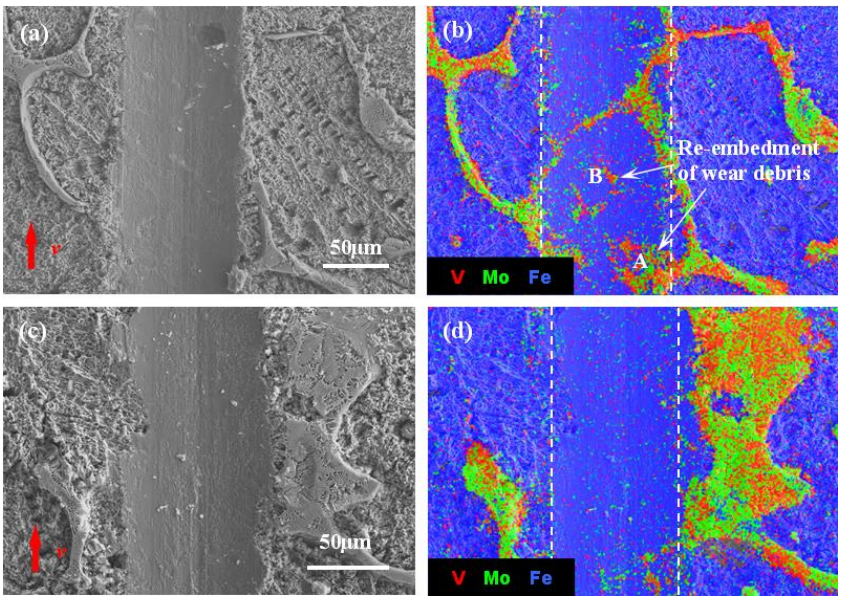

Fig.11 (a), (c) SEM images and (b), (d) EDS face analyses of eutectic carbides within the scratch groove at

15N (deep-etched).

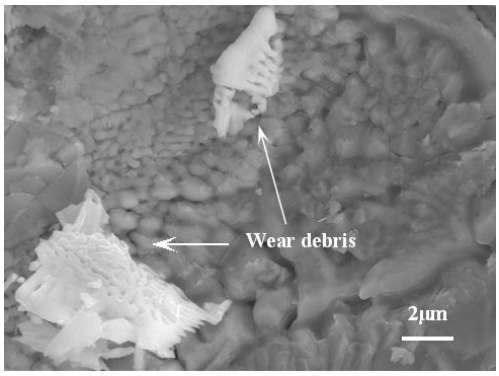

Fig.12 Morphology of wear debris of eutectic carbides within the scratch groove at 20N (deep-etched).

4 Discussion

4.1 Wear mechanism of the eutectic carbide with matrix protection

Fig.13 schematically illustrates the wear mechanism of the eutectic carbide with matrix protection. During a single-pass scratch test, the diamond indenter acted as a hard particle drags across the soft specimen. The normalforce F_N and tangential force F_T along the sliding direction both work on the surface forming the scratch, some of the materials is separated from the workpiece becoming wear debris. The eutectic carbide, which are embedded in the matrix, is also being cut off. Therefore, micro-cutting is the main wear mechanism of the eutectic carbide.

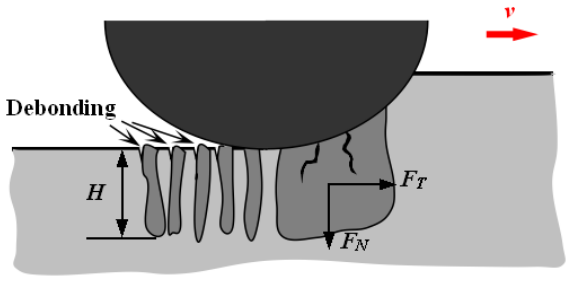

Fig.13 Wear mechanism of eutectic carbide with protection of matrix.

From Fig.13, when the resultant force associated from the F_T is larger than the bond strength between the eutectic carbide and matrix, the carbide dendrites debond from the matrix, and form intergranular cracks, this is one potential wear mechanisms of the

eutectic carbide. The intergranular cracks between the eutectic carbide and matrix have also been observed in Fig.5-Fig.7. When F_T causes a resultant stress over the ultimate strength of the eutectic carbide, brittle fracture occurs and transgranular cracks initiate inside the carbide dendrite, this is another wear mechanisms of the eutectic carbide. If the intergranular and transgranular cracks propagate and intersect with each other, the fractured carbide particles will fall off and become wear debris. Generally, the ultimate strength of the eutectic carbide itself is larger than the bond strength between the eutectic carbide and matrix. So the intergranular cracks are more likely to initiate under a lower load. As the load increases, the transgranular and intergranular cracks co-exist within the eutectic region, which is evident in the cracks shown in Fig5.(b)-(c). It is reasonable to deduced that, the main operating wear mechanism of the eutectic carbide includes micro-cutting, brittle fracture and debonding from the matrix. The brittle fracture of the eutectic carbide leads to the formation of transgranular cracks, while the debonding from the matrix causes the formation of intergranular cracks.

4.1.1 Effect of the eutectic carbide orientation and morphology

The wear mechanism of the eutectic carbide is also related with the orientation and morphology of the carbide dendrite. Mostly, the carbide dendrites embeded in the matrix are strip-shaped structure from two-dimensional observation. From Fig.14(a), when the dendrite length is parallel to the sliding direction of the indenter, the dendrite width d is only 0.3-0.7μm. The relatively smaller force area $S=dH$ (H is defined in Fig.13) could lead to a larger stress $\sigma = F_T / S$ on each point of the carbide surface, which make it easy to reach/exceed the ultimate strength of the eutectic carbide and bond strength between the eutectic carbide and matrix, so that both the transgranular and intergranular cracks could form. As illustrated in Fig.14(b), if the dendrite length is perpendicular to the sliding direction of the indenter, the dendrite length l is within several dozens of microns, the larger force area $S=lH$ lead to smaller stress σ, which make it relatively easier to reach the bond strength

between the eutectic carbide and matrix, so the intergranular cracks will dominate . In the transition zone between the carbide clusters, the carbide dendrites are mainly bulk-like shape from two-dimensional observation (see Fig.14(c)). The moment of the bulk-like carbide dendrite $F_T \times D$ from Fig.14(c) is obviously smaller than that of the strip dendrite $F_T \times l$ (the situation illustrated in Fig.14(a)), so it is difficult to initiate transgranular cracks within the bulk-like dendrites. Therefore, in addition to micro-cutting, another wear mechanism of the eutectic carbideis the carbide debonding from the matrix (Fig.14(b)-(c)).

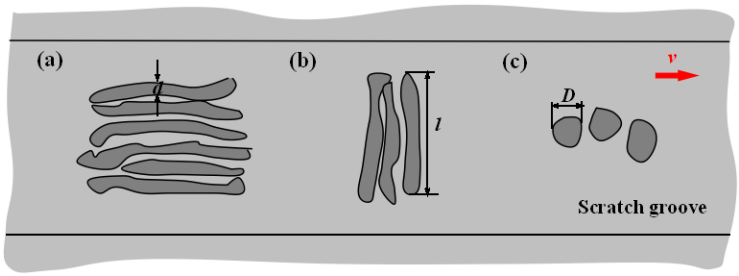

Fig.14 Effects of orientation and two-dimentional morphology on wear mechanism of eutectic carbide: (a) strip-like, the carbide length is parallel to scratch direction; (b) strip-like, the carbide length is perpendicular to scratch direction; (c) bulk-like.

4.1.2 Effect of the eutectic carbide type

In this alloy, the eutectic carbide contains eutectic MC and M_2C. From SEM observation, the way a crack initiates n and propagates within the eutectic region are also found to be related with the carbide type. Fig.15 shows a schematic diagram of crack initiation and propagation in eutectic MC and M_2C. Generally, transgranular crack or intergranular crack firstly occurs in a dendrite with a single type of carbides. From Fig.15(a), due to the larger dendrite width and spacing, as well as the non-parallel-arrangement between the carbide dendrites in the same cluster, the transgranular and intergranular cracks within eutectic MC are not in a straight line, this made it difficult for the cracks to propagate. From Fig.15(b), in eutectic M_2C, if the dendrite length is parallel to the sliding direction as shown in Fig.14(a), the transgranular cracks tend to initiate in a single dendrite and propagate into the cluster. The spacing of the eutectic M_2C dendrite is small thus offers lower resistance for the propagation

of cracks on adjecnt carbides feather. In addition, the transgranular cracks in each carbide feather within the M_2C cluster is along a similar direction, these conditions would make it easier for the crack connect and propagate across the carbide dendrite, which could reach to a length of several dendrite width. From Fig.15(c), the intergranular cracks could easily initiate in the transition zone between M_2C clusters but hardly propagate because of the irregular dendrite distribution and variation in the dendrite spacing, both which would stop or deflect the crack path and prevent it from propogation. At grain boundary and on the edge of M_2C cluster, the large intergranular crack (several microns long and up to 1μm wide) can be found as shown in Fig.15(d). Generally,this type of crack can form only when the carbide boundary is approximately perpendicular to the scratch direction..

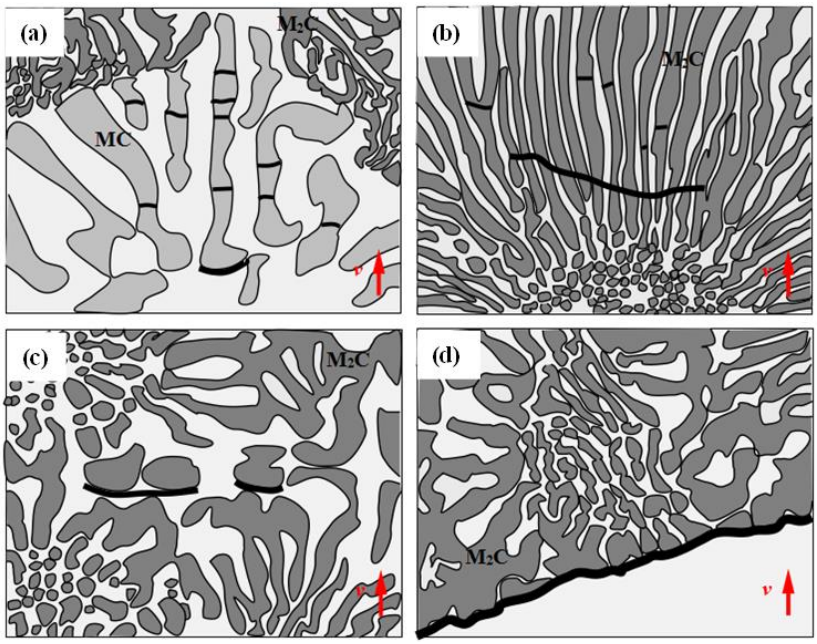

Fig.15 Schematic diagram of crack initiation and propagation for (a) eutectic MC and (b)-(d) eutectic M_2C.

An interesting finding from the observation on the fracture pattern of eutectic M_2C, the eutectic MC is that the eutectic MC can be more effective to prevent crack propagation. This offers an improved informed understanding on the influence of morphology and distribution of eutectic carbides on thewear resistance as well as hardness [26-28]. Since eutectic MC

offers better fracture and wear resistance than eutectic M_2C, how to minimize or control the eutectic M_2C would be of great industrial significance. It is known from Fig.2(c) and 2(d) that eutectic MC is a V-rich carbide, while eutectic M_2C is rich in element Mo. So V content can be increased and Mo content can be reduced appropriately to obtain more eutectic MC and less M_2C, and thus improve the mechanical properties of the alloy. In addition, eutectic MC and M_2C forms simultaneously in the eutectic reaction, and their dendritic morphologies can be observed by fast cooling treatment (water quenching) from high temperature. If the cooling rate is reduced after the eutectic reaction, the eutectic carbides, especially eutectic M_2C would grow up, and its dendritic morphology with small dendrite spacing and parallel dendrite arrangement would disappear and form coarsened block-shape structure similar to eutectic MC, which would be more effective in preventing crack propagation.

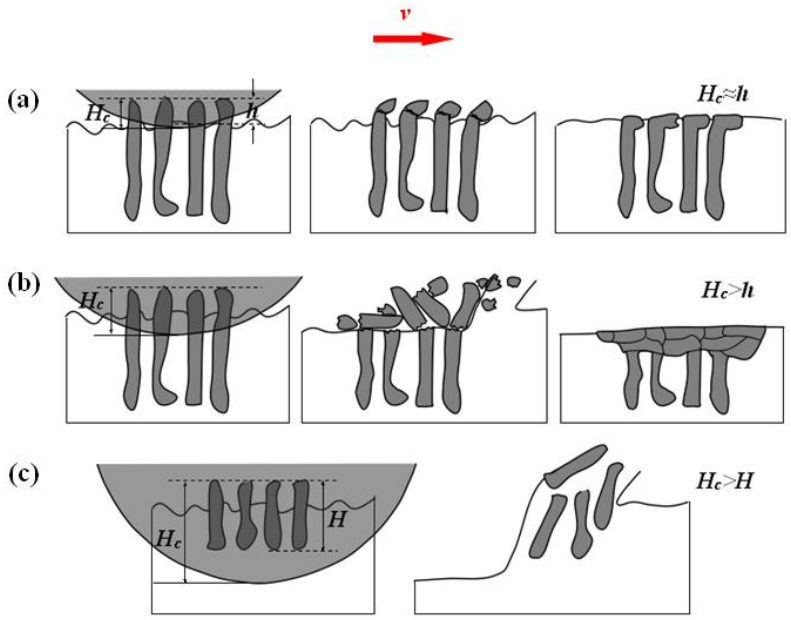

Fig.16 Wear mechanism of eutectic carbide without protection of matrix: (a) $H_c \approx h$; (b) $H_c > h$; (c) $H_c > H$.

4.2 Wear mechanism of the eutectic carbide without matrix protection

Fig.16 schematically illustrates the wear mechanisms of the eutectic carbide without matrix protection. From Fig.16(a), when the load is relatively small, the indentation depth H_c is comparable to the height h, which represents the extent the carbide dendrites bulged out of

the matrix after deep-etching. The bulged dendrites break off under the force F_T to become wear debris and re-embedded into the matrix next to the original carbides under the function of F_N. As observed in Fig.9(b), under this fracture mechanism, the dendrite width would increase resulting in dendrites partly connected with each other. As the load increases, when H_c is larger than h, as shown in Fig.16(b), a much large amount broken dendrites forms, some part of these carbide fragments is re-embed in the matrix near the fracture site, while other wear debris be displaced by the indenter in the wear system and move to and re-embedded into other location of matrix as referred by Area B in Fig.11(b). Fig.16(c) shows the case when H_c is larger than the dendrite length H, under this condition, the eutectic carbide is cut off from the roots and becomes part of the wear debris on the cluster scale, as shown in Fig.14.

4.3 Interaction between matrix and eutectic carbide

The observation and analyses above illustrate that the matrix and eutectic carbide interacted with each other through a complex mechanism during a scratch process, which directly influence the energy dispersion, fracture and wear of carbides. Firstly, the matrix can effectively relieve the high internal stress within the eutectic region by means of the plastic deformation, thus delay/reduce the crack initiation. Moreover, with protection from the matrix, only transgranular and intergranular cracks are observed; while without the protection matrix, carbide dendrites could easily break off and become wear debris in the scratch groove. This suggests that matrix plays the support and protective role in eutectic carbide. In addition, due to the plastic deformation and high toughness of matrix itself, the cracks within the carbide dendrite hardly extend into the matrix indicating that matrix can effectively prevent the crack propagation. Because of the relative high hardnessand dendrite aggregation , the indenter suffers larger resistance in eutectic carbide than the matrix, resulting in a smaller indentation depth. This make the eutectic carbide still slightly higher than the matrix

vertically under the indenter. In this case, the matrix in the eutectic region is not fully in contact with the indenter force, which offers, to certain extent, a form of protection on the matrix by the protruding eutectic carbides. In addition, the carbide debris of different sizes (either on the dendrite or cluster scale) will be re-embedded into the matrix eventually, in other words, the matrix on the surface will be partially covered by carbide debris with higher hardness and, possibly lower friction coefficients, which can effectively improve the wear resistance.

5 Conclusion

Studies of the single-point abrasive wear of eutectic carbides in a Fe-Cr-W-Mo-V-C alloy were conducted using diamond point scratch testing on as polished and deep etched samples to establish a more detailed understanding on the fracture and wear mode of eutectic carbides . The following conclusions could be made:

1) When a surrounding matrix is present, the slip-lines appear in scratch edges of the matrix phase, and micro-cracks initiate from the eutectic structure. The micro-cracks are mainly transgranular cracks in eutectic MC with limited coalescence and propagation. While the transgranular cracks and intergranular cracks coexist in eutectic M_2C, and propagate within or across the carbide clusters pending on the normal load applied

2) The main operating wear mechanism of the eutectic carbide includes micro-cutting, brittle fracture and debonding from the matrix. The brittle fracture of the eutectic carbide causes the initiation of transgranular cracks, while the debonding from the matrix causes the initiation of the intergranular cracks. The wear mechanism is also influenced by the morphology, dendrite orientation and type of the eutectic carbide.

3) Scratch tests on deep etched samples showed that, without matrix protection, the carbide dendrites break off and form wear debris during the wear process. When indentation depth is larger than the dendrite length, the carbide dendrites are cut off from the roots and

forms wear debris on the cluster scale in dimension.

Acknowledgements

The authors would like to express their gratitude for projects supported by National Natural Science Foundation of China (51271163) and National Natural Science Foundation of China (51471148).

Reference

[1] J. Guo, B. Liao, L.G. Liu, Q. Li, X.J. Ren, Q.X. Yang, Forging limit of a novel high-speed-steel cold work roll based on ductile fracture criteria by finite element model, Mater. Des. 52 (2013) 1027–1034.

[2] M. Nilsson, M. Olsson, Microstructural, mechanical and tribological characterisation of roll materials for the finishing stands of the hot strip mill for steel rolling, Wear 307 (2013) 209–217.

[3] H.C. Li, Z.Y. Jiang, A.K. Tieu, W.H. Sun, D.B. Wei, Experimental study on wear and friction of work roll material with 4% Cr and added Ti in cold rolling, Wear 271 (2011) 2500–2511.

[4] D.W. Yi, J.D. Xing, Z.Y. Zhang, H.G. Fu, C.Y. Yang, Effect of titanium and nitrogen additions on the microstructures and three-body abrasive wear behaviors of Fe–B cast alloys, Tribol. Lett. 50 (2013) 439–448.

[5] C. Katsich, E. Badisch, Effect of carbide degradation in a Ni–based hardfacing under abrasive and combined impact/abrasive conditions, Surf. Coat. Tech. 206 (2011) 1062–1068.

[6] J. Guo, Q. Li, H.W. Qu, L.G. Liu, Q.X. Yang, Carbide precipitation behavior and wear resistance of a novel roller steel, J.Mater. Eng. Perform. 22 (2012) 1790–1797.

[7] A. Muthuraja, S. Senthilvelan, Abrasive wear performance of tungsten carbide based self-lubricant cutting tool material, Inter. J. Refract. Met. H. 51 (2015) 91–101.

[8] E.G. Moghaddam, N. Karimzadeh, N. Varahram, P. Davami, Investigation of the effect of tungsten substitution on microstructure and abrasive wear performance of in situ VC–reinforced high-manganese austenitic steel matrix composite, Metall. Mater. Trans. A 44 (2013) 3826–3835.

[9] C.K.N. Oliveira, R.M. Muñoz Riofano, L.C. Casteletti, Micro-abrasive wear test of niobium carbide layers produced on AISI H13 and M2 steels, Surf. Coat. Tech. 200 (2006) 5140–5144.

[10] L.S. Zhong, F.X. Ye, Y.H. Xu, J.S. Li, Microstructure and abrasive wear characteristics of in situ vanadium carbide particulate–reinforced iron matrix composites, Mater. Des. 54 (2014) 564–569.

[11] Y.P. Ji, S.J. Wu, L.J. Xu, Y. Li, S.Z. Wei, Effect of carbon contents on dry sliding wear behavior of high vanadium high speed steel, Wear 294–295 (2012) 239–245.

[12] A. Bedolla-Jacuinde, F.V. Guerra, I. Mejía, J. Zuno-Silva, M. Rainforth, Abrasive wear of V–Nb–Ti alloyed high–chromium white irons, Wear 332-333 (2015) 1006–1011.

[13] C. Rodenburg, W.M. Rainforth, A quantitative analysis of the influence of carbides size distributions on wear behaviour of high-speed steel in dry rolling/sliding contact, Acta Mater. 55 (2007) 2443–2454.

[14] J.J. Coronado, Effect of load and carbide orientation on abrasive wear resistance of white cast iron, Wear 270 (2011) 823–827.

[15] R.J. Chung, X. Tang, D.Y. Li, B. Hinckley, K. Dolman, Microstructure refinement of hypereutectic high Cr cast irons using hard carbide–forming elements for improved wear resistance, Wear 301 (2013) 695–706.

[16] K. Van Acker, D. Vanhoyweghen, R. Persoons, J. Vangrunderbeek, Influence of tungsten carbide particle size and distribution on the wear resistanceof laser clad WC/Ni coatings, Wear 258 (2005) 194–202.

[17] S.R Wang, L.H. Song, Y. Qiao,M. Wang, Effect of carbide orientation on impact-abrasive wear resistance of high–Cr iron used in shot blast machine, Tribol. Lett. 50 (2013) 439–448.

[18] J. Guo, L.G. Liu, Q. Li, Y.L. Sun, Y.K. Gao, X.J. Ren, Q.X. Yang, Characterization on carbide of a novel steel for cold work roll during solidification process, Mater. Charact. 79 (2013) 100–109.

[19] H.F. Fischmeister, R. Riedl, S. Karagoz, Solidification of high–speed tool steels, Metall. Trans. A 20A (1989) 2133–2148.

[20] A. Tauqir, H. Nowotny, P.R. Strutt, Studies of carbides in a rapidly solidified high–speed steel, Metall. Trans. A 21A (1990) 3021–3026.

[21] B. Attard, A. Matthews, A. Leyland, G. Cassar, Enhanced surface performance of Ti–6Al–4V alloy using a novel duplex process combining PVD–Al coating and triode plasma oxidation, Surf. Coat. Tech. 257 (2014) 154–164.

[22] J.L. Mo, M.H. Zhu, A. Leyland, A. Matthews, Impact wear and abrasion resistance of CrN, AlCrN and AlTiN PVD coatings, Surf. Coat. Tech. 215 (2013) 170–177.

[23] G. Cassar, J.C. Avelar-Batista Wilson, S. Banfield, J. Housden, A. Matthews, A. Leyland, Surface modification of Ti–6Al–4V alloys using triode plasma oxidation treatments, Surf. Coat. Tech. 206 (2012) 4553–4561.

[24] L.A. Dobrzanski, Melting and crystallization behavior of W–V–Si high–speed steels, Steel Res. 57 (1986) 37–45.

[25] G.L.F. Powell, P.G. Lloyd, A deep etching technique for the examination of the carbide of high chromium cast iron in a scanning electron microscope, Metallography 14(1981) 271–274.

[26] H.K. Kim, J.I. Park, J.H. Ryu, Correlation of microstructure and thermal–fatigue properties of centrifugally cast high–speed steel rolls, Metall. Mater. Trans. 35A (2004) 481–492.

[27] G. Byun, S. Oh, C.G. Lee, Correlation of microstructure and microstructure mechanism of five work rolls, Metall. Mater. Trans. 30A (1999) 234–243.

[28] S.J. Oh, S.J. Kwon, H. Oh, Phase analysis of two steel work rolls using mossbauer spectroscopy, Metall. Mater. Trans. 31A (2000) 793–798.